JPE 16-4-29

http://dx.doi.org/10.6113/JPE.2016.16.4.1551
ISSN(Print): 1598-2092 / ISSN(Online): 2093-4718

Flexible Voltage Support Control with Imbalance Mitigation Capability for Inverter-Based Distributed Generation Power Plants under Grid Faults

Yuewu Wang†, Ping Yang*, and Zhirong Xu**

†School of Electric Power, South China University of Technology, Guangzhou, China
*Guangdong Key Laboratory of Clean Energy Technology, South China University of Technology, Guangzhou, China
**National-Local Joint Engineering Laboratory for Wind Power Control and Integration Technology, South China University of Technology, Guangzhou, China

Abstract

The high penetration level of inverter-based distributed generation (DG) power plants is challenging the low-voltage ride-through requirements, especially under unbalanced voltage sags. Recently, a flexible injection of both positive- (PS) and negative-sequence (NS) reactive currents has been suggested for the next generation of grid codes. This can enhance the ancillary services for voltage support at the point of common coupling (PCC). In light of this, considering distant grid faults that occur in a mainly inductive grid, this paper proposes a complete voltage support control scheme for the interface inverters of medium or high-rated DG power plants. The first contribution is the development of a reactive current reference generator combining PS and NS, with a feature to increase the PS voltage and simultaneously decrease the NS voltage, to mitigate voltage imbalance. The second contribution is the design of a voltage support control loop with two flexible PCC voltage set points, which can ensure continuous operation within the limits required in grid codes. In addition, a current saturation strategy is also considered for deep voltage sags to avoid overcurrent protection. Finally, simulation and experimental results are presented to validate the effectiveness of the proposed control scheme.

Key words: Distributed generation, Low-voltage ride-through, Positive and negative sequence current control, Voltage sag, Voltage support

I. INTRODUCTION

With the rapidly growing installation of renewable energy resources and distributed generation (DG) power plants, such as wind farms and photovoltaic parks, grid-connected inverters have been widely utilized [1]-[3]. The behaviors of these interface inverters become critical to the stability and reliability of the power system, and lead to new challenges in the requirements for ancillary services. One of the most important issues is how to withstand and provide uninterrupted service in the face of short-term grid disturbances, especially under unbalanced voltage sags caused by distant grid faults.

Different national grid codes [4]-[6] provided by transmission system operators dictate the behavior of inverter-based DG power plants under voltage sags, where low-voltage ride-through (LVRT) capability is a mandatory function. Depending on the depth and duration of a voltage sag at the point of common coupling (PCC), the present grid code requirements demand the DG plants to stay connected and provide voltage support by the injection of reactive current into the grid. To accomplish this aim, interface inverters first need to avoid their own overvoltage and overcurrent protection due to the sag, and then inject the required reactive current. However, the major requirements just consider reactive current

Manuscript received Oct. 5, 2015; accepted Apr. 4, 2016
Recommended for publication by Associate Editor Kyeon Hur.
†Corresponding Author: myth-pluto@163.com
Tel: +86-15099956175, South China University of Technology
*Guangdong Key Laboratory of Clean Energy Technology, South China University of Technology, China
**National-Local Joint Engineering Laboratory for Wind Power Control and Integration Technology, South China University of Technology, China

via positive sequence (PS). This raises the PS voltage, but has no influence on the negative sequence (NS) voltage. Moreover, these requirements do not take into account the shape of the voltage sag. They only consider the PS voltage amplitude or the root mean square (rms) voltage. Thus, under the unbalanced voltage sags caused by distant grid faults, if the inductive grid impedance and the plant rated power are large enough, all of the PCC phase voltages are raised equally, leading to a risk of triggering overvoltage protection in the non-fault phase(s) and causing disconnection of the system [7]. For better fulfillment of the ride-through operation, the suggested requirements in the next generation of grid codes could demand a flexible injection of both PS and NS reactive currents to enhance ancillary services.

Many advanced control algorithms have been proposed to meet the LVRT requirements and to simultaneously optimize the overall system performance under various grid faults [8]–[14]. In [8] and [9], active and reactive power oscillations can be flexibly controlled through different system constraints. In [10] and [11], trade-offs between power fluctuations and current harmonics are provided to achieve adjustable power quality. In [12]-[14], fluctuations of the dc-link voltage in two-stage systems are attenuated to maintain safe operation. However, all of these studies mainly focus on achieving particular control objectives, leaving the same risk of triggering overvoltage protection in the non-fault phase(s).

To further improve voltage support services, some recent studies have dealt with the injection of both PS and NS currents via other control algorithms, for the purpose of restoring PCC voltages to within their limits for continuous operation. As a preliminary study, the significant contribution presented in [7] is the introduction of a new open-loop control algorithm for reference current generation, which provides a variable control parameter to modify the voltage support strategy. Based on [7], extended studies [15]-[20] have developed various voltage support control loops. A closed-loop voltage control scheme is proposed in [15] where online values for the reactive power and the control parameter are provided, although limited to some specific voltage sags. For proper operation under any type of voltage sag, the authors in [16] and [17] proposed two improved reactive power/current injection schemes for high-power and low-power rating DG sources, respectively. However, all of the schemes designed in [15]-[17] need to be integrated with the grid impedance and to assume the knowledge of its value, even if it is actually variable related to the fault position and requires an extra grid impedance estimator. To avoid such limitations and to keep the injected currents within safety limits during unbalanced voltage sags, several remarkable control strategies have been developed in [18]-[20]. In [18], the introduced reactive power control scheme can effectively accomplish the voltage support task independently of the grid impedance, but it still leaves a non-negligible voltage imbalance. In [19] and [20], fully flexible injections of positive and negative active and reactive powers are included. However, the authors are more concerned with the maximization of the inverter power capacity and do not take into account voltage limits for continuous operation, leading to a lack of effective decision on voltage support in some scenarios. In addition, a very interesting voltage support scheme with a safe predefined ampere constraint in its current injection is developed in [21], despite the fact that it works in an open-loop way.

Thus, under distant grid faults occurring in a mainly inductive grid, the topic of voltage support control is still open for further research. In this paper, a complete voltage support control scheme for medium or high-rated inverter-based DG power plants is proposed. Compared to some existing control strategies [15]-[17], the proposed scheme is independent of grid impedance and does not require any extra estimation of it [22]. Therefore, the complexity of the algorithm is reduced. Unlike [18], imbalance mitigation is one of the major aims of this paper. In order to raise the PS voltage and simultaneously reduce the NS one at the PCC, a reactive current reference generator is designed via a combination of both PS and NS currents. In order to properly restore the PCC voltages to within the limits for continuous operation under unbalanced voltage sags, a new voltage support control loop is proposed, with two flexible PCC voltage set points calculated on-line. Furthermore, a current saturation strategy is included, with the priority of injecting PS current while avoiding overcurrent if the sag depth exceeds the capability of the inverter.

This paper is organized as follows. Section II formulates the problem. Section III designs a current reference generator and proposes a voltage support control loop with the current saturation strategy. Two PCC voltage set points are also derived. Section IV and section V validate the proposed control scheme by means of simulation and experimental results, respectively. Section VI is the conclusion.

II. Problem Formulation

This study focuses on the voltage support capability of interface inverters in medium or high-rated DG power plants. This section begins with a description of a typical DG power plant architecture in the power system. Then, the propagation of voltage sags through cascade-connected transformers is summarized and the sag characterization is mathematically analyzed. Finally, control objectives are formulated to flexibly support the grid voltage during faults.

A. DG Power Plant in Power System

Besides power inverters supplying active and reactive power to the grid, a typical DG power plant also includes static synchronous compensators (STATCOMs), switched capacitors and local loads. STATCOMs are employed for power quality improvements, such as voltage regulation, network balance, and some dynamic reactive power compensation, while

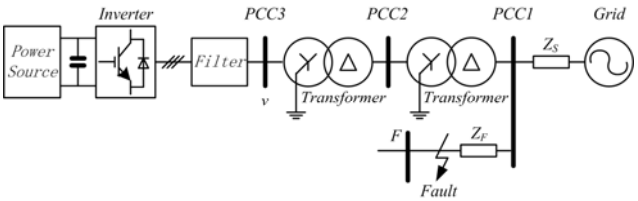

Fig. 1. Simplified configuration of a DG power plant.

TABLE I
VOLTAGE SAGS PROPAGATION DUE TO *DY* TRANSFORMERS

	Point of common coupling		
Fault type	PCC1	PCC2	PCC3
Three-phase	A	A	A
Single-phase to ground	B	C	D
Two-phase	C	D	C
Two-phase to ground	E	F	G

switched capacitors are operated to provide steady-state compensation. Since power inverters act as the key interface to deliver power to the electrical grid, a simplified architecture of a DG power plant connected to an electrical grid is shown in Fig. 1. As the main form of a DG power plant, wind farm or photovoltaic park model is composed of power sources, inverters, filters and step-up transformers. Through two *Dy* transformers, the plant is connected to a high-voltage grid at the PCC1.

Under normal grid conditions, the maximum active power and some required reactive power with a high power quality are injected into the grid. Whenever a voltage sag occurs along with a grid fault, grid codes force the DG plant to remain connected within an established time, and huge amounts of reactive power are dictated for voltage support [23], [24]. If a grid fault occurs near the PCC1, the DG plant has little effect on the voltage support, and just delivers the required reactive current. However, for distant grid faults, transmission and distribution networks with a high *X/R* ratio are mainly inductive. Once the rated power of the plant is large enough, the voltage can be effectively supported by a flexible injection of reactive current, and ride-through capability with a minimum voltage limit becomes possible.

B. Voltage Sag Propagation and Characterization

Grid faults, such as phase-to-ground short circuit, phase-to-phase short circuit and start-up of large motors, may cause voltage sags, presenting PS, NS and zero-sequence (ZS) components. The nature of a sag depends on the number of phases affected by the grid fault, the transformer connections and the fault point. In this paper, the voltage *v* at the PCC3 in Fig. 1 is of concern. It is propagated from the original voltage sags existing at the PCC1 as a result of different types of faults occurring at bus F. A classification of the four types of voltage sags occurring at the PCC1 is proposed in [25], and the new types appearing at the PCC2 and PCC3 are discussed in [26]. Taking into account the cascade connection of two *Dy* transformers, the origin and propagation of different types of voltage sags are classified in Table I, as summarized in [27].

In this paper, the voltage sags (types A, C, D and G) at the PCC3 are investigated for voltage support, with the ZS component removed by a *Dy* transformer. Using the Clarke transformation, the instantaneous phase voltages *v* at the PCC3 can be expressed in the $\alpha\beta$ stationary reference frame as:

$$\begin{bmatrix} v_\alpha \\ v_\beta \end{bmatrix} = \frac{1}{3}\begin{bmatrix} 2 & -1 & -1 \\ 0 & \sqrt{3} & -\sqrt{3} \end{bmatrix}\begin{bmatrix} v_a \\ v_b \\ v_c \end{bmatrix}. \tag{1}$$

Separated into PS and NS symmetrical components yields:

$$v_\alpha = v_\alpha^+ + v_\alpha^- \tag{2}$$

$$v_\beta = v_\beta^+ + v_\beta^- \tag{3}$$

where v_α^+, v_β^+ and v_α^-, v_β^- denote the instantaneous PS and NS voltages in the $\alpha\beta$ frame, respectively.

Considering the amplitude, frequency and initial angle, the voltage components can be represented as:

$$v_\alpha^+ = V^+ \cos(\omega t + \varphi^+) \tag{4}$$

$$v_\beta^+ = V^+ \sin(\omega t + \varphi^+) \tag{5}$$

$$v_\alpha^- = V^- \cos(-\omega t - \varphi^-) \tag{6}$$

$$v_\beta^- = V^- \sin(-\omega t - \varphi^-) \tag{7}$$

where V^+ and V^- are the amplitudes of the PS and NS; ω is the grid angular frequency; and φ^+ and $-\varphi^-$ are the initial phase angles of the PS and NS.

Based on (4)-(7), the angle $\varphi = \varphi^+ - \varphi^-$ between the PS and NS can be calculated as follows:

$$\cos(\varphi) = \frac{v_\alpha^+ v_\alpha^- - v_\beta^+ v_\beta^-}{V^+ V^-} \tag{8}$$

$$\sin(\varphi) = \frac{v_\alpha^+ v_\beta^- + v_\beta^+ v_\alpha^-}{V^+ V^-}. \tag{9}$$

Under unbalanced voltage sags conditions, an effective parameter for evaluating the voltage variation is the voltage unbalance factor, *n* [28]. This factor represents the ratio of the NS voltage to the PS voltage. It can be expressed as:

$$n = \frac{V^-}{V^+}. \tag{10}$$

Under normal grid conditions, the unbalance factor is rather small, whenever being kept below 0.02-0.03 is acceptable [29]. However, it can experience a high value during unbalanced voltage sags. And it is objective that this factor can only partially characterize the voltage sag, without any phase angle information. But it is still enough to derive the proposed set points, which will be analyzed in Section III.

C. Voltage Support Control Objectives

In the following, the behavior of a three-phase inverter in a DG plant is described to explain the voltage support concept.

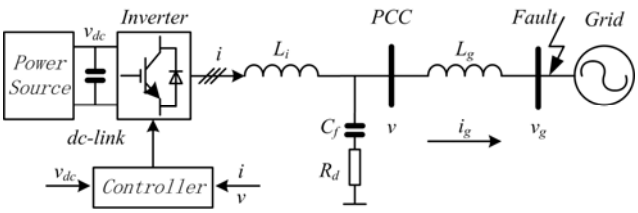

Fig. 2. Diagram of three-phase grid-connected inverter.

Focusing on the inverter, instead of the one in Fig. 1, a more simplified grid-connected configuration is presented in Fig. 2. The inverter is connected to the PCC through an *LC* filter with a passive damping resistor in series with the capacitor. In addition, the inductance L_g represents the equivalent grid impedance of step-up transformers and transmission networks. In order to properly support the PCC voltage under grid faults, typical LVRT curves with voltage profiles are strictly defined in national grid codes [4]-[6]. With the existence of grid impedance L_g, reactive current can be flexibly injected to achieve voltage support at the PCC with different control objectives [7]. For continuous operation to ride through grid faults, there is a safety voltage limits region in which the amplitudes of the phase voltages are restricted. The lower limit is 0.9 per unit (p.u.) of the nominal voltage, while the upper limit is 1.1 p.u. [6]. During a balanced voltage sag (type A), it is obvious that all of the phase voltages should be raised equally above the lower limit, depending only on the injection of PS reactive current. On the other hand, whenever unbalanced voltage sags (type C, D and G) occur, the minimum phase voltage should be regulated to the lower limit while the maximum limit is not permitted to exceed the upper limit. Under such a condition, a flexible combination of both PS and NS reactive currents is necessary [7], [21].

For unbalanced voltage sags, a phasor diagram can be used to explain the voltage support concept [16], [30], as illustrated in Fig. 3. The grid voltage phasor V_g at the fault point is decomposed into PS and NS: V_g^+, PS voltage phasor rotating with the positive direction at ω rad/s and whose initial phase angle is φ^+, and V_g^-, NS voltage phasor rotating with the negative direction at $-\omega$ rad/s and whose initial phase angle is $-\varphi^-$. By flowing through the grid impedance L_g, a 90° PS current I_g^+ lagging from V_g^+ produces an orthogonal voltage $\omega L_g I_g^+$, which helps to increase the amplitude of the PS voltage V^+ at the PCC with respect to the fault voltage V_g^+. On the other hand, a 90° NS current I_g^- leading from V_g^- produces an orthogonal voltage $\omega L_g I_g^-$, which helps to reduce the amplitude of the NS

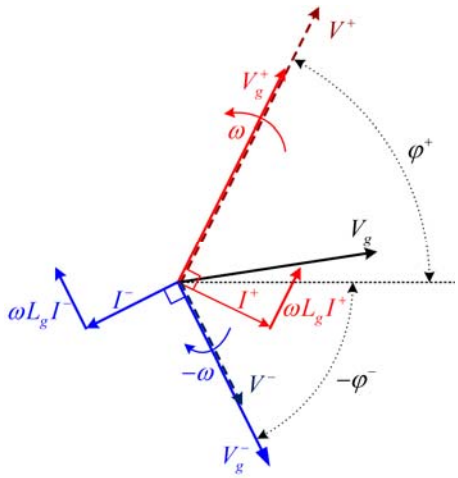

Fig. 3. Phasor diagram of voltage support.

voltage V^- at the PCC with respect to the fault voltage V_g^-. An amplitude increment of V^+ at the PCC can boost all of the PCC phase voltages until the minimum one exceeds the lower voltage limit. At the same time, a reduction of V^- leads to a smaller voltage unbalance factor, which means that the voltage imbalance is mitigated to avoid overvoltage.

Thus, by flexibly combining both PS and NS currents, and by considering the phase voltage amplitudes V_a, V_b, and V_c at the PCC, the control objectives to achieve voltage support under grid faults can be formulated as:

$$\begin{aligned} &\text{find} \quad I_g^+, I_g^- \\ &\text{such that}: \quad \max\{V_a, V_b, V_c\} \le 1.1 \text{ p.u.} \\ &\qquad\qquad \min\{V_a, V_b, V_c\} \ge 0.9 \text{ p.u..} \end{aligned} \tag{11}$$

The solution to accomplish the control objectives mainly consists of two cascaded parts. The inner part is a reactive current reference generator, which produces appropriate PS and NS reference currents depending on their amplitudes provided by the outer part. In addition, the outer part is a new voltage support control loop possessing two flexible PCC voltage set points calculated within the upper and lower limits. In this paper, the active current carrying the maximum or the command power is delivered to feed the grid under normal grid conditions. Whenever voltage sags occur, to achieve a better voltage support, only an injection of reactive current is considered by the proposed solution, since the present requirements do not specify the amount of active current during faults [6]. A detailed fulfillment of the solution is presented in the following section.

III. Proposed Voltage Support Control Scheme

This section develops the step-by-step procedure to achieve the whole control scheme for voltage support under grid faults. First, the system topology and control structure are described

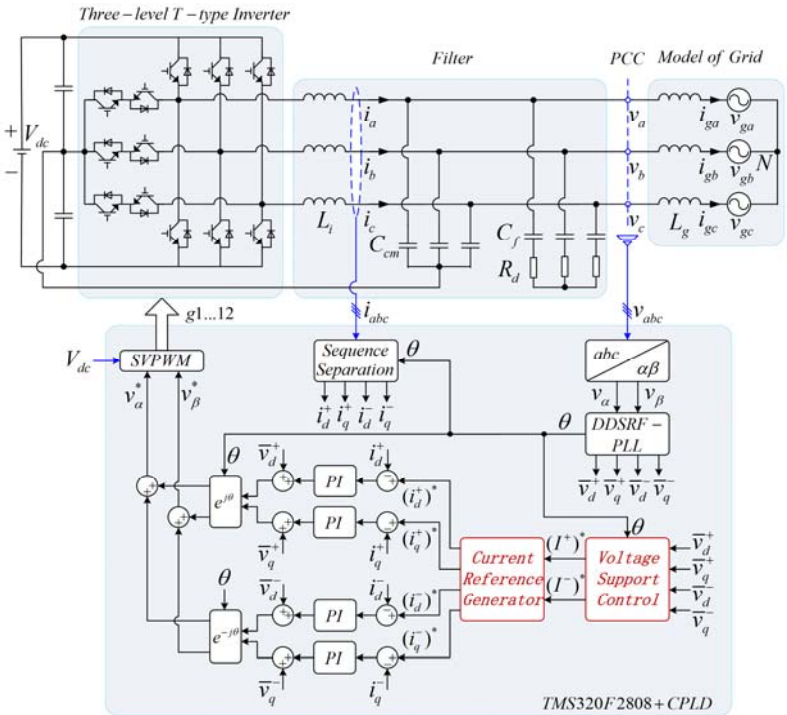

Fig. 4. System configuration and control structure.

with fundamental analysis. Then, the proposed reactive current references for PS and NS are derived. In addition, a new voltage support control loop is devised to provide the amplitudes of PS and NS currents. This is accomplished with a current saturation strategy to limit the maximum injected current to the rated one. Finally, to complete the ride-through operation, two flexible PCC voltage set points dynamically adjusted by the voltage unbalance factor are developed. They can mitigate the voltage imbalance to an acceptable level.

A. System Description and Control Structure

The detailed system configuration of the investigated three-phase grid-connected inverter in a DG plant is shown in Fig. 4, which is composed of a power source, a dc-link capacitor, an inverter, a filter and a grid. The power source instead of a renewable source provides a constant dc-link voltage, in order to focus the analysis on the inverter side control. Instead of a conventional three-level neutral point clamped (NPC) inverter, a three-level T-type inverter is employed, which is especially efficient and a real alternative for medium switching frequency low-voltage applications [31]. The inverter is connected to the grid at the PCC through an *LC* filter. The capacitor of the *LC* filter is divided into two parts, where the common point of the smaller part (C_{cm}) is linked to the neutral point of the input split capacitors to reduce the leakage current in transformerless structures [32]. In addition, to avoid a possible resonance problem, a damping resistor R_d is used in series with the larger part C_f . Finally, the inductance L_g is used to model the equivalent impedance between the PCC and the grid, and the grid is emulated by a programmable ac source.

In addition, as shown in Fig. 4, the voltages and currents of the power stage are measured to achieve voltage support control under grid faults. The inputs of the control system are the measured phase voltages v_{abc} at the PCC, the inverter side currents i_{abc} , and the dc-link voltage V_{dc} . The control system is implemented in the double synchronous reference frame, including the voltage support control block, the current reference generator and two inner fast current loops. For proper grid synchronization under unbalanced voltage sags, a stable decoupled double synchronous reference frame phase-locked loop (DDSRF-PLL) [33] is adopted to align the d^+ axis of the positive reference frame dq^+ with the PS voltage. The DDSRF has a sequence separation feature that can extract and separate the PS and NS components of voltage and current at the PCC. i_d^+ , i_q^+ and i_d^- , i_q^- represent the PS and NS currents, respectively. Similarly, $\overline{v}_d^+$, $\overline{v}_q^+$ and $\overline{v}_d^-$, $\overline{v}_q^-$ represent the PS and NS voltages filtered by the low-pass filter, respectively. With the obtained PS and NS voltage components, the proposed voltage support control loop and current reference generator are developed, which will be explained in the following subsections. Then, the PS and NS current references are controlled individually through dual vector current controllers (DVCCs) [8], [34]. However, the

cross-decoupling terms are neglected because these terms would cancel each other when the same technique is implemented in the opposite-sequence reference frame [35]. Additionally, space vector pulse width modulation (SVPWM) is used for the dc-link neutral-point voltage balance and for driving signal generation. However, this subject is beyond the scope of this paper.

B. Current References for Positive and Negative Sequences

Note that the PLL is controlling the angular position θ of the dq^+ frame. Thus, $\overline{v}_q^+$ is forced to be equal to zero, and $\overline{v}_d^+$ is equal to the PS voltage amplitude V^+:

$$V^+ = \overline{v}_d^+. \tag{12}$$

However, both $\overline{v}_d^-$ and $\overline{v}_q^-$ can take any arbitrary value depending on the relative angular position between the PS and NS voltages.

Under normal grid conditions, the NS current references $(i_d^-)^*$ and $(i_q^-)^*$ are always set to zero, for a balanced current injection. Meanwhile, the PS active current reference $(i_d^+)^* = 0.33 I_{\max}$ is considered to simulate the generated power, where $I_{\max}$ is the amplitude of the rated current; and the PS reactive current reference $(i_q^+)^*$ is set to compensate the *LC* filter phase shift for a unity power factor on the grid side [36].

Under grid faults, as already explained at the end of Section II, only reactive current is injected in this case. Furthermore, the inverter side currents i_{abc} are sensed for control purposes instead of the grid side currents formulated in (11). Since the d^+ axis is aligned with the PS voltage, for a 90° PS current lagging from the PS voltage in the dq^+ frame to increase V^+, $(i_d^+)^*$ and $(i_q^+)^*$ are directly expressed as:

$$(i_d^+)^* = 0 \tag{13}$$

$$(i_q^+)^* = -(I^+)^* \tag{14}$$

where $(I^+)^*$ is the amplitude reference of the PS current offered by the voltage support control loop. On the other hand, for a 90° NS current leading from the NS voltage in the opposite-sequence dq^- frame to reduce V^-, by applying the rotation matrix, $(i_d^-)^*$ and $(i_q^-)^*$ can be deduced as:

$$\begin{bmatrix} (i_d^-)^* \\ (i_q^-)^* \end{bmatrix} = (I^-)^* \begin{bmatrix} \cos(\pi/2) & \sin(\pi/2) \\ -\sin(\pi/2) & \cos(\pi/2) \end{bmatrix} \begin{bmatrix} \dfrac{\overline{v}_d^-}{V^-} \\ \dfrac{\overline{v}_q^-}{V^-} \end{bmatrix} \tag{15}$$

yielding:

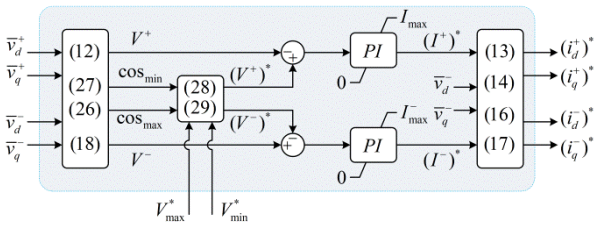

Fig. 5. Diagram of the proposed voltage support control.

$$(i_d^-)^* = (I^-)^* \left(\frac{\overline{v}_q^-}{V^-}\right) \tag{16}$$

$$(i_q^-)^* = (I^-)^* \left(-\frac{\overline{v}_d^-}{V^-}\right) \tag{17}$$

where $(I^-)^*$ is the amplitude reference of the NS current generated by the voltage support control loop, and the NS voltage amplitude V^- can be calculated as:

$$V^- = \sqrt{(\overline{v}_d^-)^2 + (\overline{v}_q^-)^2}. \tag{18}$$

C. Voltage Support With Current Saturation

The aim of this subsection is to design a voltage support control loop that provides the amplitude references $(I^+)^*$ and $(I^-)^*$ according to the PCC voltage set points $V_{\max}^*$ and $V_{\min}^*$, as shown in Fig. 5.

Based on the discussion at the end of Section II, it can be seen that, an increment of the amplitude V^+ is proportional to the reference $(I^+)^*$, while a reduction of amplitude V^- is proportional to the reference $(I^-)^*$. Thus, a PI regulator that produces the value of the reference $(I^+)^*$, can be employed to regulate V^+ to the reference $(V^+)^*$. Similarly, another PI regulator that produces the value of the reference $(I^-)^*$, is employed to regulate V^- to the reference $(V^-)^*$. Note that the initial $(V^-)^*$ is always set to be smaller than the initial V^- to achieve NS voltage reduction and imbalance mitigation. Therefore, the sign of the error between the reference and the feedback is opposite to that of the PS. In addition, two current saturation limits $I_{\max}$ and $I_{\max}^-$ are added to the two regulators, to ensure safe operation of the inverter.

In summary, to complete the implementation of the proposed voltage support control, three derivations need to be done: $I_{\max}^-$, the current saturation limit for the NS regulator; $(V^+)^*$ and $(V^-)^*$, the amplitude references for the PS and NS voltages related to the PCC voltage set points $V_{\max}^*$ and $V_{\min}^*$; and $V_{\max}^*$ and $V_{\min}^*$, the flexible PCC voltage set points

between the upper and lower limits. The last derivation will be carried out in the next subsection, while the first two are derived in the following.

By applying the inverse Clarke transformation to (4)-(7), the amplitude of the phase voltages in the *abc* natural reference frame can be written as:

$$V_a = \sqrt{(V^+)^2 + (V^-)^2 + 2V^+V^-\cos(\varphi)} \quad (19)$$

$$V_b = \sqrt{(V^+)^2 + (V^-)^2 + 2V^+V^-\cos(\varphi + 2\pi/3)} \quad (20)$$

$$V_c = \sqrt{(V^+)^2 + (V^-)^2 + 2V^+V^-\cos(\varphi + 4\pi/3)} \quad (21)$$

where $\cos(\varphi)$ is calculated in (8), and $\cos(\varphi + 2\pi/3)$ and $\cos(\varphi + 4\pi/3)$ can be deduced from (8) and (9).

Note that the PS and NS voltage components in (8) and (9) are expressed in the $\alpha\beta$ frame. Thus, using the inverse Park transformation results in:

$$\begin{bmatrix} v_\alpha^+ \\ v_\beta^+ \end{bmatrix} = \begin{bmatrix} \cos(\theta) & -\sin(\theta) \\ \sin(\theta) & \cos(\theta) \end{bmatrix} \begin{bmatrix} \overline{v}_d^+ \\ \overline{v}_q^+ \end{bmatrix} \quad (22)$$

$$\begin{bmatrix} v_\alpha^- \\ v_\beta^- \end{bmatrix} = \begin{bmatrix} \cos(\theta) & \sin(\theta) \\ -\sin(\theta) & \cos(\theta) \end{bmatrix} \begin{bmatrix} \overline{v}_d^- \\ \overline{v}_q^- \end{bmatrix}. \quad (23)$$

From expressions (19)-(21), only two of them are of interest. Defining $V_{\max}$ and $V_{\min}$ as the maximum and minimum amplitudes of the phase voltages results in:

$$V_{\max} = \sqrt{(V^+)^2 + (V^-)^2 + 2V^+V^-\cos_{\max}} \quad (24)$$

$$V_{\min} = \sqrt{(V^+)^2 + (V^-)^2 + 2V^+V^-\cos_{\min}} \quad (25)$$

where the cosine functions $\cos_{\max}$ and $\cos_{\min}$ are:

$$\cos_{\max} = \max\{\cos(\varphi), \cos(\varphi + 2\pi/3), \cos(\varphi + 4\pi/3)\} \quad (26)$$

$$\cos_{\min} = \min\{\cos(\varphi), \cos(\varphi + 2\pi/3), \cos(\varphi + 4\pi/3)\}. \quad (27)$$

From (24) and (25), it can be clearly seen that the PS and NS voltage amplitudes are related to the phase voltage amplitudes. Thus, the references $(V^+)^*$ and $(V^-)^*$ can be obtained from the PCC voltage set points $V_{\max}^*$ and $V_{\min}^*$ as follows:

$$(V^+)^* = \sqrt{\frac{\mu + \sqrt{\mu^2 - [(V_{\max}^*)^2 - (V_{\min}^*)^2]^2}}{2(\cos_{\max} - \cos_{\min})}} \quad (28)$$

$$(V^-)^* = \frac{(V_{\max}^*)^2 - (V_{\min}^*)^2}{2(\cos_{\max} - \cos_{\min})(V^+)^*} \quad (29)$$

where

$$\mu = (V_{\min}^*)^2\cos_{\max} - (V_{\max}^*)^2\cos_{\min}. \quad (30)$$

So far, the above discussion assumes that the control objectives formulated in (11) can be achieved absolutely. However, in the case of deep voltage sags or a DG plant with a small contribution to the total power of the grid, a higher reactive current is required for voltage support. In this case, it is possible that the required reactive current could exceed the maximum amplitude of the rated current $I_{\max}$. Therefore, a current saturation strategy is necessary, and that proposal in [21] is extended to design the current saturation strategy in this paper.

Note that the proposed voltage support control in Fig. 5 gives priority to the PS PI regulator to regulate V^+. Therefore, the PS reference $(I^+)^*$ is identified first, and it can be used to deduce the NS current saturation limit $I_{\max}^-$. In particular, if the voltage sag is so deep that the PS regulator is limited to the rated current amplitude $I_{\max}$, $I_{\max}^-$ for the NS regulator has to be adjusted to zero. As a result, only PS reactive current is injected.

It is designed so that the phase currents are fast enough to follow their references. Thus, the PS and NS currents are 90º lagging and 90º leading with respect to their corresponding sequence voltages, respectively. According to (4)-(7), the PS and NS currents in the $\alpha\beta$ frame are obtained as:

$$i_\alpha^+ = I^+\cos(\omega t + \varphi^+ - \pi/2) \quad (31)$$

$$i_\beta^+ = I^+\sin(\omega t + \varphi^+ - \pi/2) \quad (32)$$

$$i_\alpha^- = I^-\cos(-\omega t - \varphi^- - \pi/2) \quad (33)$$

$$i_\beta^- = I^-\sin(-\omega t - \varphi^- - \pi/2) \quad (34)$$

Like (19)-(21), by using the inverse Clarke transformation on (31)-(34), the amplitudes of the phase currents are expressed as:

$$I_a = \sqrt{(I^+)^2 + (I^-)^2 + 2I^+I^-\cos(\varphi_I)} \quad (35)$$

$$I_b = \sqrt{(I^+)^2 + (I^-)^2 + 2I^+I^-\cos(\varphi_I + 2\pi/3)} \quad (36)$$

$$I_c = \sqrt{(I^+)^2 + (I^-)^2 + 2I^+I^-\cos(\varphi_I + 4\pi/3)} \quad (37)$$

where $\varphi_I = (\varphi^+ - \pi/2) - (\varphi^- + \pi/2) = \varphi - \pi$. Depending on the value of φ, the maximum current amplitude occurs in different phases. According to the conclusion presented in [21], with the obtainment of the reference $(I^+)^*$, the saturation limit $I_{\max}^-$ for the NS regulator can be calculated as follows.

For $0 \le \varphi < (2\pi/3)$, I_b is the maximum. Thus:

$$I_b = \sqrt{(I^+)^2 + (I^-)^2 + 2I^+I^-\cos(\varphi - \pi + 2\pi/3)} \le I_{\max} \quad (38)$$

then:

$$I_{\max}^- = (I^+)^*\cos(\varphi + 2\pi/3) + \sqrt{[(I^+)^*]^2[\cos^2(\varphi + 2\pi/3) - 1] + I_{\max}^2}. \quad (39)$$

For $(2\pi/3) \le \varphi < (4\pi/3)$, I_a is the maximum. Thus:

$$I_a = \sqrt{(I^+)^2 + (I^-)^2 + 2I^+I^-\cos(\varphi - \pi)} \le I_{\max} \quad (40)$$

then:

$$I_{\max}^- = (I^+)^*\cos(\varphi) + \sqrt{[(I^+)^*]^2[\cos^2(\varphi) - 1] + I_{\max}^2}. \quad (41)$$

For $(4\pi/3) \le \varphi < 2\pi$, I_c is the maximum. Thus:

$$I_c = \sqrt{(I^+)^2 + (I^-)^2 + 2I^+I^-\cos(\varphi - \pi + 4\pi/3)} \leq I_{\max} \quad (42)$$

then:

$$I^-_{\max} = (I^+)^* \cos(\varphi + 4\pi/3) + \sqrt{[(I^+)^*]^2[\cos^2(\varphi + 4\pi/3) - 1] + I^2_{\max}}. \quad (43)$$

D. PCC Voltage Set Points for Continuous Operation

As previously explained, for the completion of the proposed voltage support control shown in Fig. 5, the last step is to devise the two PCC voltage set points $V^*_{\max}$ and $V^*_{\min}$.

In [18], considering the grid nominal voltage V_{nom} and the limits for continuous operation, two basic strategies for the PCC voltage set points are discussed. To make a small modification, the first strategy is formulated as:

$$V^*_{\max} = 1.02V_{nom} \quad (44)$$

$$V^*_{\min} = 0.98V_{nom}. \quad (45)$$

And the second strategy is formulated as:

$$V^*_{\max} = 1.10V_{nom} \quad (46)$$

$$V^*_{\min} = 0.90V_{nom}. \quad (47)$$

Obviously, the first strategy requires a high reactive current injection to simultaneously raise all of the phase voltages and greatly remove the voltage imbalance. Under unbalanced voltage sags with a significant voltage imbalance, the second strategy is simple and suitable for a continuous operation. However, it runs short of flexibility and there is still a considerable voltage imbalance. Therefore, in this paper, by integrating the voltage unbalance factor *n*, a flexible strategy is proposed to dynamically adjust the PCC voltage set points.

The original conception for the proposed voltage set points can be expressed as:

$$V^*_{\max} = (1.02 + k_1 n)V_{nom} \quad (48)$$

$$V^*_{\min} = (0.98 - k_1 n)V_{nom} \quad (49)$$

where k_1 is a proportional term gain and is set to 0.35. At the beginning of the voltage sags, a large unbalance factor *n* results in saturation of the two set points within the limits defined in (46) and (47). In addition, the adaptive features of the two set points ensure a reduction in the factor *n*. Under the regulation of the proposed voltage support control, the factor *n* becomes smaller and smaller, leading to a smaller $V^*_{\max}$ near $1.02V_{nom}$ and a larger $V^*_{\min}$ near $0.98V_{nom}$. As a result, the two dynamical voltage set points can be viewed as an intermediate solution between the first and the second strategy. Furthermore, in order to inject a smaller amount of reactive current, the final strategy for the proposed voltage set points is chosen as:

$$V^*_{\max} = (1.02 + k_2 n)V^*_{\min} \quad (50)$$

$$V^*_{\min} = 0.90V_{nom} \quad (51)$$

TABLE II
KEY PARAMETERS OF THE SYSTEM

Symbol	Description	Nominal Value
S_b	inverter rated power (base power)	30 kVA, 1 pu
V_{nom}	grid nominal voltage (l-n, peak)	$230\sqrt{2}$ V, 1 pu
$I_{\max}$	inverter rated current amplitude	61.49 A, 1 pu
f_g	grid frequency (base frequency)	50 Hz, 1 pu
V_{dc}	dc-link voltage	685 V, 2.106 pu
L_i	LC inverter side inductances	0.7 mH, 0.042 pu
C_{cm}	LC common capacitors	3.3 μF, 0.005 pu
C_f	LC filter capacitors	30 μF, 0.049 pu
R_d	LC damping resistors	1 Ω, 0.189 pu
L_g	grid line inductances	3.4 mH, 0.206 pu
f_s	switching/control frequency	16 kHz, 320 pu

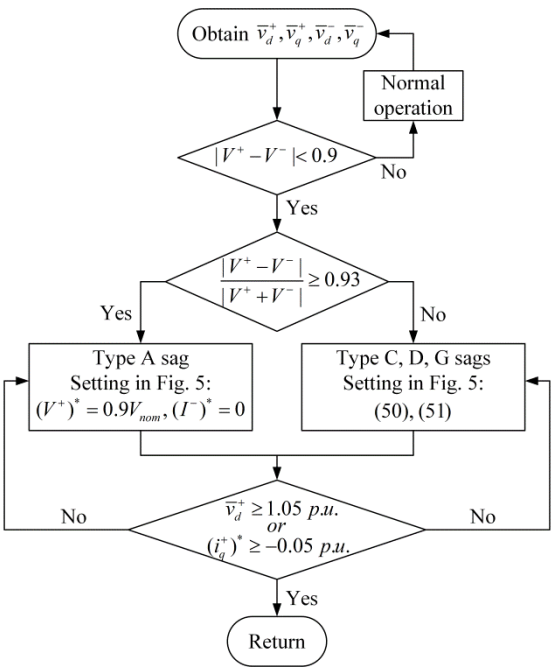

Fig. 6. Flowchart of the proposed control scheme.

where k_2 is a proportional term gain and is set to 1. Thus, the minimum phase voltage can be regulated to the low boundary value, and the voltage unbalance factor can be reduced to an acceptable one. This can also be flexibly adjusted, by changing $V^*_{\max}$ according to the variable parameter k_2 presented in (50).

IV. SIMULATION RESULTS

Based on the system configuration in Fig. 4, a model of a 30 kW single-stage three-phase three-level grid-connected inverter system was implemented in the MATLAB/Simulink

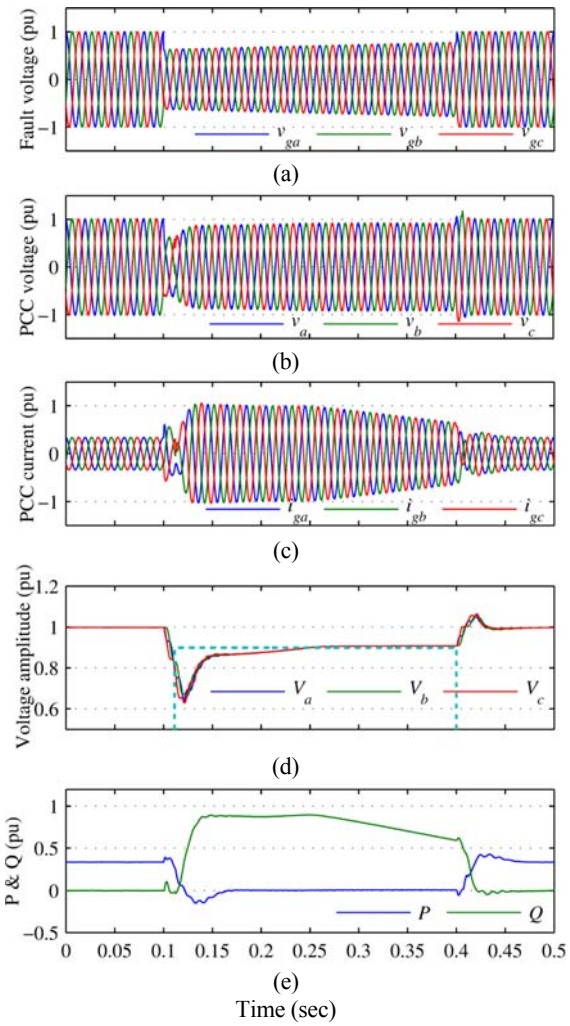

Fig. 7. Simulation results under type A voltage sag.

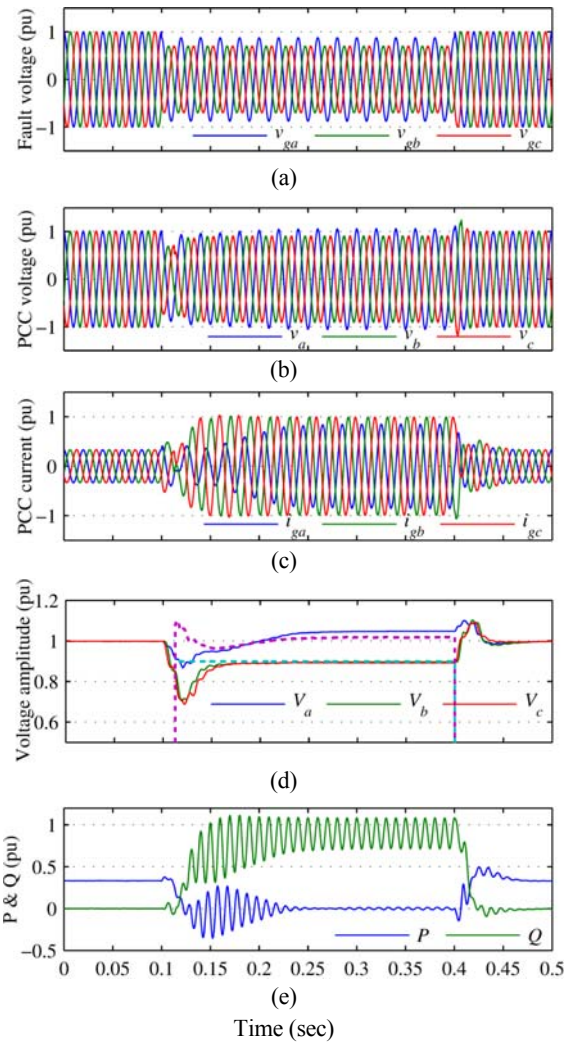

Fig. 8. Simulation results under type G voltage sag.

environment. The nominal values for the key parameters of the system are listed in Table II. Due to the limit on the rated power, a grid equivalent inductance $L_g = 3.4\,\text{mH}$ between the PCC and the grid was used for voltage support. The DDSRF-PLL, the voltage support control, the current reference generator, the inner current loops and the SVPWM were all executed once per switching period, this is consistent with the coming experimental implementation. In addition, the sag detector presented in [37] has been employed to determine the occurrence and the sag type of voltage sags. Including balanced voltage sags (type A), the flowchart to carry out the entire control scheme is depicted in Fig. 6. Note that only PS reactive current is needed under a type A sag.

According to [27], taking into account the effect of transformers, only four types of voltage sags (types A, C, D and G) occur at the PCC. Of these, type A and type G have been tested to validate the proposed voltage support control in the simulation environment. The sag characterizations and the sequential behaviors of the fault voltage for the test are given in Table III [38]. They are presented in per-unit values. Before and after the sag, 0.33 p.u. of PS active current is delivered to feed the grid. This is acting as the DG source behavior. During the sag (from time t = 0.1 to 0.4 s), the proposed control is activated and only reactive current is injected.

A. Type A Voltage Sag

Fig. 7 shows detailed simulation results under a type A voltage sag. The sag profile of the grid fault voltage is depicted in Fig. 7(a), where a balanced voltage sag occurs at t = 0.1 s with a duration of 0.3 s, and recovers from 0.63 p.u. to 0.78 p.u. Before the voltage sag, the system runs under normal operation, delivering balanced current and active power only [see Fig. 7(c) and (e)]. When the sag takes place at t = 0.1 s, with a 10 ms delay for proper detection of the sag type, the proposed voltage support control is activated. As can be observed in Fig. 7(b), the three phase voltages at the PCC are equally boosted. At the beginning, the sag is so deep that the reactive current at the PCC increases greatly and is saturated by the PS regulator described in Fig. 5, without exceeding the maximum limit (1 p.u.) [see Fig. 7(c)]. Fig. 7(d) clearly shows the effect of the voltage support control during the dynamic sag. The voltage amplitudes at the PCC are raised finitely by the

TABLE III
TYPE A AND TYPE G VOLTAGE SAGS FOR SIMULATION

		Time		
		0~0.1 s	0.1~0.4 s	0.4~0.5 s
Type A	v_{ga}	$1\angle 0°$	$(0.63 \sim 0.78)\angle 0°$	$1\angle 0°$
	v_{gb}	$1\angle -120°$	$(0.63 \sim 0.78)\angle -120°$	$1\angle -120°$
	v_{gc}	$1\angle 120°$	$(0.63 \sim 0.78)\angle 120°$	$1\angle 120°$
Type G	v_{ga}	$1\angle 0°$	$0.88\angle 0°$	$1\angle 0°$
	v_{gb}	$1\angle -120°$	$0.70\angle -128.8°$	$1\angle -120°$
	v_{gc}	$1\angle 120°$	$0.70\angle 128.8°$	$1\angle 120°$

TABLE IV
TYPE C AND TYPE D VOLTAGE SAGS FOR EXPERIMENT

		Time		
		0~0.1 s	0.1~0.4 s	0.4~0.5 s
Type C	v_{ga}	$1\angle 0°$	$1\angle 0°$	$1\angle 0°$
	v_{gb}	$1\angle -120°$	$0.85\angle -125.8°$	$1\angle -120°$
	v_{gc}	$1\angle 120°$	$0.85\angle 125.8°$	$1\angle 120°$
Type D	v_{ga}	$1\angle 0°$	$0.80\angle 0°$	$1\angle 0°$
	v_{gb}	$1\angle -120°$	$0.95\angle -114.8°$	$1\angle -120°$
	v_{gc}	$1\angle 120°$	$0.95\angle 114.8°$	$1\angle 120°$

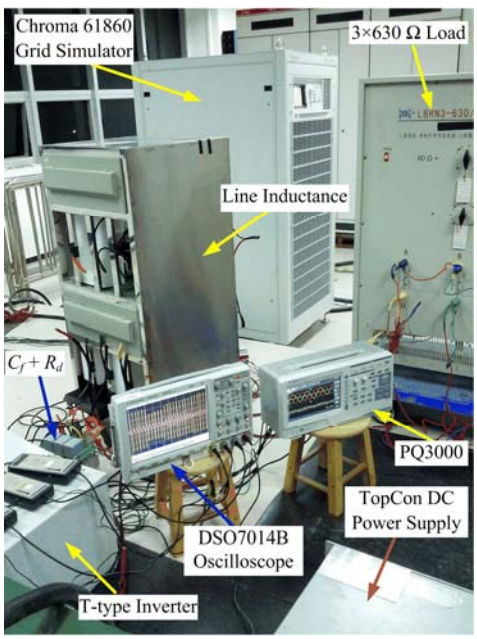

Fig. 9. The experimental setup.

saturated reactive current, and they increase gradually along with the recovery of the fault voltage. Whenever the voltage amplitudes reach the lower limit (0.9 p.u. in the dotted line) and become stabilized at it, the reactive current exits the saturation and decreases step by step. Finally, at t = 0.4 s, the sag disappears and the system returns to normal operation. It can be seen that, before, during, and after the sag, no oscillations appear in either the instantaneous active or reactive power [see Fig. 7(e)] since no imbalance exists in a type A voltage sag.

B. Type G Voltage Sag

Fig. 8 shows simulation results under a type G voltage sag. Unlike a type A sag, a type G sag presents a significant imbalance. In this case, a specified and constant sag depth [see Table III and Fig. 8(a)] is selected to evaluate the current saturation strategy during the unbalanced voltage sag. In Fig. 8(d), after the activation of the proposed control, the two lower phase voltages are regulated to 0.9 p.u., while the upper phase voltage is finally maintained at a certain value above the designed value [in the higher dotted line, dynamically calculated online according to (50)], meaning that the two expected set points are only partly achieved. As depicted in Fig. 8(c), the maximum PCC current amplitude can be limited to 1 p.u., which shows that the current saturation strategy can comply with the safety limit. On the other hand, the limited and unbalanced current shows that the PS voltage amplitude reference can be tracked satisfactorily, while the NS voltage amplitude reference is saturated by $I_{\max}^{-}$ as described in Fig. 5, as a result of the designed priority of the PS regulator. Throughout the sag, an oscillation at twice the fundamental grid frequency appears in both the instantaneous active and reactive power due to the unbalanced voltage sag.

V. EXPERIMENTAL RESULTS

To further validate the proposed control scheme, a 30kW laboratory prototype with the same parameters listed in Table II was built. A photograph of the experimental setup is shown in Fig. 9. The DG source behavior was emulated by a TopCon programmable DC power supply. The utility grid was emulated by a Chroma 61860 regenerative grid simulator with a Y-connected 630 Ω/phase local load. It was connected to the inverter through a line inductance. The measurement instruments consisted of a ZLG PQ3000 power quality analyzer and an Agilent DSO7014B oscilloscope. The control algorithm was implemented in a Texas Instruments fixed-point digital signal processor (DSP) TMS320F2808. The 12 driving signals were generated by a complex programmable logic device (CPLD) coordinating with the DSP.

As a continuation of the simulation, in the experimental validation, the remaining type C and type D voltage sags have been programmed in the grid simulator, with the detail given in Table IV [38]. Like the simulation, a 0.33 p.u. PS active current is injected under normal operation while only reactive current is considered during the voltage sag. However, when a

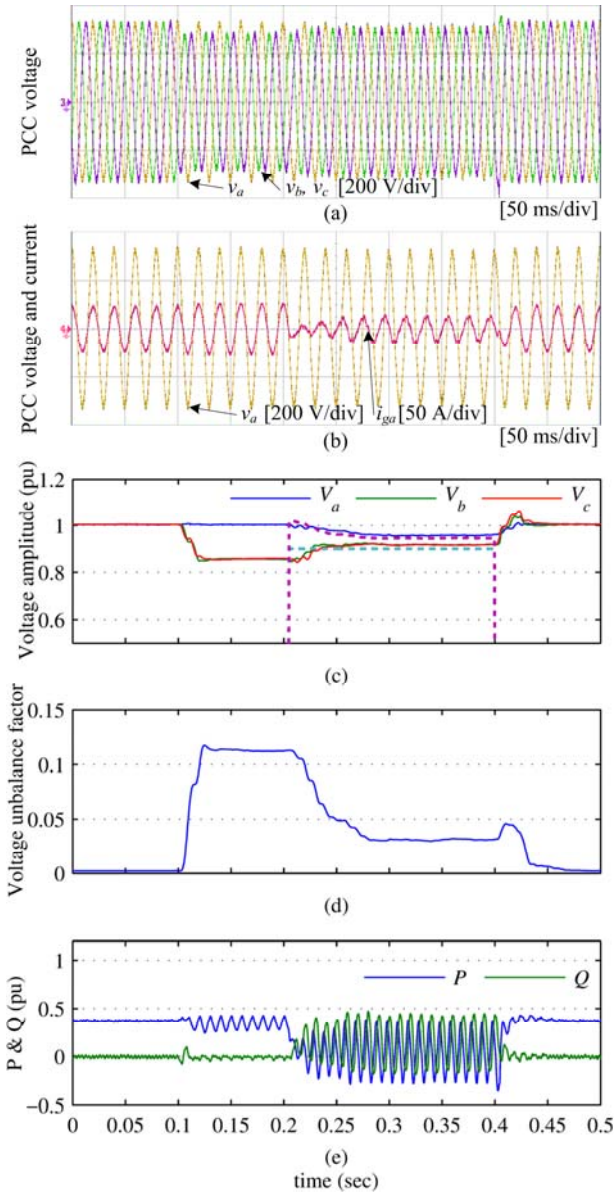

Fig. 10. Experimental results under type C voltage sag.

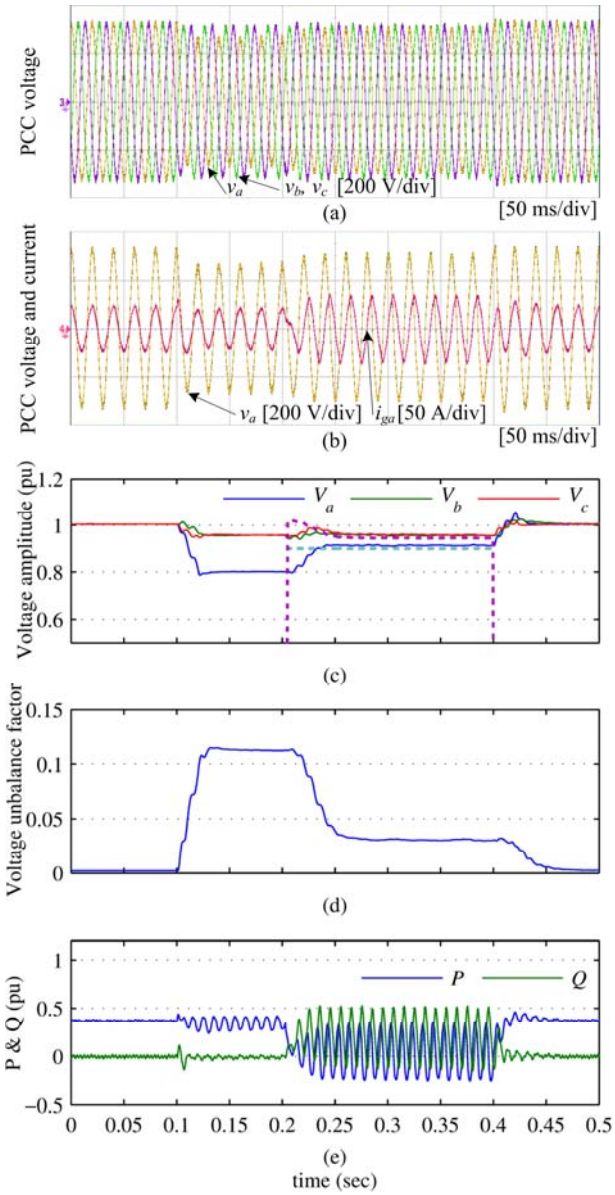

Fig. 11. Experimental results under type D voltage sag.

sag occurs, a 0.1 s delay to activate the proposed control is adopted to clearly show the voltage sag profile.

A. Type C Voltage Sag

Fig. 10 shows experimental results under a type C voltage sag. Fig. 10(a) and (b) are the PCC voltage and current measured by the DSO7014B, and Fig. 10(c)-(e) shows the results computed in MATLAB/Simulink, based on the original data recorded by the PQ3000. As stated previously, from t = 0.1 to 0.2 s, the voltage support control is not enabled, and the waveforms and amplitudes of the sag voltage at the PCC can be clearly observed in Fig. 10(a) and (c), respectively. Moreover, during this time interval, it should be pointed out that, in addition to the PS active current, a small amount of NS current is specified and injected to eliminate the reactive power oscillation [see Fig. 10(e)] that could affect the PCC voltage amplitudes. After the startup of the proposed control, in Fig. 10(c), the two dropped voltages rise to 0.9 p.u., and the non-dropped (phase a) tracks the dynamical set point. Both of them possess an acceptable deviation meeting the main objective of the proposed control scheme. Meanwhile, in Fig. 10(b), the PCC current i_{ga} becomes almost 90° leading the PCC voltage v_a, which draws a capacitive reactive power in phase a in accordance with the reduction of the voltage amplitude V_a; in Fig. 10(d), the voltage unbalance factor is reduced from 0.112 to 0.031; in Fig. 10(e), a significant oscillation appears in both the instantaneous active and reactive power due to the imbalance in the system.

B. Type D Voltage Sag

Fig. 11 shows the experimental results under a type D

voltage sag. Like type C sags, as the main objective of the proposed control scheme, the voltage amplitudes in Fig. 11(c) acceptably track the two set points; and the voltage unbalance factor in Fig. 11(d) is reduced from 0.113 to 0.030. In addition, active and reactive power oscillations are also present as expected. However, in Fig. 11(b), the PCC current i_{ga} becomes almost 90° lagging the PCC voltage v_a, which draws an inductive reactive power in phase *a* to support the voltage amplitude V_a.

C. Computational Load

Note that the proposed control contains some division and square root operations, the control system is implemented in a fixed-point DSP, and it is necessary to confirm the computational load of the algorithm execution. For optimizing the execution speed, the highest clock frequency of 100 MHz is chosen to clock the TMS320F2808. Then the Texas Instruments TMS320C28x IQmath Library is adopted to provide highly optimized and high precision mathematical functions. Finally, the key code sections are copied from the internal flash memory to the internal random access memory (RAM) at run time. This is done in order to achieve zero wait-states for maximum speed. Under normal operation, the measured algorithm execution time is 26.5 μs, including the analog-to-digital converter, the DDSRF-PLL, the sequence separation, the inner current loops and the SVPWM. When the proposed voltage support control (without the current saturation strategy) is activated, the execution time suffers an increase of 19.3μs, resulting in an idle time of 26.7% of the switching period, which is acceptable for the entire control algorithm.

VI. Conclusion

This paper presented a complete voltage support control scheme for inverter-based DG power plants under the voltage sags caused by grid faults. The main contribution of this paper consists of a reactive current reference generator and a voltage support control loop. A detailed analysis indicates that the current reference generator has a feature to increase the PS voltage and to simultaneously decrease the NS voltage. Under a balanced voltage sag, all of the PCC phase voltages are equally raised to the minimum limit for continuous operation. This is accomplished solely by the PS regulator designed in the voltage support control loop. Under unbalanced voltage sags, two flexible PCC voltage set points within the upper and lower limits are computed online. Then the highest phase voltage and the lowest phase voltage are regulated to the two set points, with a significant reduction in the voltage unbalance factor. Furthermore, when the sag depth exceeds the capacity of the inverter, the maximum phase current can be successfully limited to the rated current via the current saturation strategy.

According to an analysis of the simulation and experimental results, it can be concluded that under grid faults, the proposed control is suitable for achieving a combination of voltage support and imbalance mitigation for medium or high-rated DG power plants, which are connected to a mainly inductive grid with a high *X/R* ratio.

Acknowledgment

The authors would like to thank the support from the National Science and Technology Support Program (2015BAA06B02), China, and the Guangdong Strategic Emerging Industry Core Technology Research Projects (2012A032300001), China.

References

[1] W. Sinsukthavorn, E. Ortjohann, A. Mohd, N. Hamsic, and D. Morton, "Control strategy for three-/four-wire-inverter-based distributed generation," *IEEE Trans. Ind. Electron.*, Vol. 59, No. 10, pp. 3890-3899, Oct. 2012.

[2] A. Teke and M. B. Latran, "Review of multifunctional inverter topologies and control schemes used in distributed generation systems," *Journal of Power Electronics*, Vol. 14, No. 2, pp. 324-340, Mar. 2014.

[3] Q. Wang, N. Zhou, and L. Ye, "Fault analysis for distribution networks with current-controlled three-phase inverter-interfaced distributed generators," *IEEE Trans. Power Del.*, Vol. 30, No. 3, pp. 1532-1542, Jun. 2015.

[4] *Grid Code-High and Extra High Voltage*, E.ON Netz GmbH, Bayreuth, Germany. 2006.

[5] Y. Bae, T.-K. Vu, and R.-Y. Kim, "Implemental control strategy for grid stabilization of grid-connected PV system based on German grid code in symmetrical low-to-medium voltage network," *IEEE Trans. Energy Convers.*, Vol. 28, No. 3, pp. 619-631, Sep. 2013.

[6] China Electricity Council, *GB/T 19964-2012 Technical Requirements for Connecting Photovoltaic Power Station to Power System*, Beijing: Standards Press of China (in Chinese). 2012.

[7] A. Camacho, M. Castilla, J. Miret, J. C. Vasquez, and E. Alarcon-Gallo, "Flexible voltage support control for three-phase distributed generation inverters under grid fault," *IEEE Trans. Ind. Electron.*, Vol. 60, No. 4, pp. 1429-1441, Apr. 2013.

[8] S. Alepuz, S. Busquets-Monge, J. Bordonau, J. A. Martinez-Velasco, C. A. Silva, J. Pontt, and J. Rodriguez, "Control strategies based on symmetrical components for grid-connected converters under voltage dips," *IEEE Trans. Ind. Electron.*, Vol. 56, No. 6, pp. 2162-2173, Jun. 2009.

[9] F. Wang, J. L. Duarte, and M. A. M. Hendrix, "Pliant active and reactive power control for grid-interactive converters under unbalanced voltage dips," *IEEE Trans. Power Electron.*, Vol. 26, No. 5, pp. 1511-1521, May 2011.

[10] X. Guo, W. Liu, X. Zhang, X. Sun, Z. Lu, and J. M. Guerrero, "Flexible control strategy for grid-connected inverter under unbalanced grid faults without PLL," *IEEE Trans. Power Electron.*, Vol. 30, No. 4, pp. 1773-1778, Apr. 2015.

[11] F. A. S. Neves, M. Carrasco, F. Mancilla-David, G. M. S. Azevedo, and V. S. Santos, "Unbalanced grid fault

ride-through control for single-stage photovoltaic inverters," *IEEE Trans. Power Electron.*, Vol. 31, No. 4, pp. 3338-3347, Apr. 2016.
[12] M. Mirhosseini, J. Pou, and V. G. Agelidis, "Single- and two-stage inverter-based grid-connected photovoltaic power plants with ride-through capability under grid faults," *IEEE Trans. Sustain. Energy*, Vol. 6, No. 3, pp. 1150-1159, Jul. 2015.
[13] F. Lin, K. Lu, T. Ke, B. Yang, and Y. Chang, "Reactive power control of three-phase grid-connected PV system during grid faults using Takagi-Sugeno-Kang probabilistic fuzzy neural network control," *IEEE Trans. Ind. Electron.*, Vol. 62, No. 9, pp. 5516-5528, Sep. 2015.
[14] G. Ding, F. Gao, H. Tian, C. Ma, M. Chen, G. He, and Y. Liu, "Adaptive dc-link voltage control of two-stage photovoltaic inverter during low voltage ride-through operation," *IEEE Trans. Power Electron.*, Vol. 31, No. 6, pp. 4182-4194, Jun. 2016.
[15] J. Miret, A. Camacho, M. Castilla, L. G. de Vicuna, and J. Matas, "Control scheme with voltage support capability for distributed generation inverters under voltage sags," *IEEE Trans. Power Electron.*, Vol. 28, No. 11, pp. 5252-5262, Nov. 2013.
[16] A. Camacho, M. Castilla, J. Miret, R. Guzman, and A. Borrell, "Reactive power control for distributed generation power plants to comply with voltage limits during grid faults," *IEEE Trans. Power Electron.*, Vol. 29, No. 11, pp. 6224-6234, Nov. 2014.
[17] J. Miret, A. Camacho, M. Castilla, J. L. García de Vicuña, and J. de la Hoz, "Reactive current injection protocol for low-power rating distributed generation sources under voltage sags," *IET Power Electron.*, Vol. 8, No. 6, pp. 879-886, 2015.
[18] M. Castilla, J. Miret, A. Camacho, J. Matas, and L. Garcia de Vicuna, "Voltage support control strategies for static synchronous compensators under unbalanced voltage sags," *IEEE Trans. Ind. Electron.*, Vol. 61, No. 2, pp. 808-820, 2014.
[19] A. Camacho, M. Castilla, J. Miret, A. Borrell, and L. G. de Vicuna, "Active and reactive power strategies with peak current limitation for distributed generation inverters during unbalanced grid faults," *IEEE Trans. Ind. Electron.*, Vol. 62, No. 3, pp. 1515-1525, Mar. 2015.
[20] J. L. Sosa, M. Castilla, J. Miret, J. Matas, and Y. A. Al-Turki, "Control strategy to maximize the power capability of PV three-phase inverters during voltage sags," *IEEE Trans. Power Electron.*, Vol. 31, No. 4, pp. 3314-3323, Apr. 2016.
[21] C.-T. Lee, C.-W. Hsu, and P.-T. Cheng, "A low-voltage ride-through technique for grid-connected converters of distributed energy resources," *IEEE Trans. Ind. Appl.*, Vol. 47, No. 4, pp. 1821-1832, Jul. 2011.
[22] N. Hoffmann and F. W. Fuchs, "Minimal invasive equivalent grid impedance estimation in inductive-resistive power networks using extended Kalman filter," *IEEE Trans. Power Electron.*, Vol. 29, No. 2, pp. 631-641, 2014.
[23] F. Iov, A. D. Hansen, P. E. Sorensen, and N. A. Cutululis, "Mapping of grid faults and grid codes," Riso National Laboratory, Technical University of Denmark, Roskilde, Denmark, Riso-R-1617(EN), Jul. 2007.
[24] Y. Yang, F. Blaabjerg, and H. Wang, "Low-voltage ride-through of single-phase transformerless photovoltaic inverters," *IEEE Trans. Ind. Appl.*, Vol. 50, No. 3, pp. 1942-1952, May 2014.
[25] M. H. J. Bollen, "Characterisation of voltage sags experienced by three-phase adjustable-speed drives," *IEEE Trans. Power Deliv.*, Vol. 12, No. 4, pp. 1666-1671, Oct. 1997.
[26] M. H. J. Bollen, *Understanding Power Quality Problems: Voltage Sags and Interruptions*. New York: IEEE Press, 2000.
[27] M. H. J. Bollen and L. D. Zhang, "Different methods for classification of three-phase unbalanced voltage dips due to faults," *Electr. Power Syst. Res.*, Vol. 66, No. 1, pp. 59-69, Jul. 2003.
[28] C.-Y. Lee, "Effects of unbalanced voltage on the operation performance of a three-phase induction motor," *IEEE Trans. Energy Convers.*, Vol. 14, No. 2, pp. 202-208, Jun. 1999.
[29] A. von Jouanne and B. Banerjee, "Assessment of voltage unbalance," *IEEE Trans. Power Deliv.*, Vol. 16, No. 4, pp. 782-790, Oct. 2001.
[30] T.-L. Lee, S.-H. Hu, and Y.-H. Chan, "D-STATCOM with positive-sequence admittance and negative-sequence conductance to mitigate voltage fluctuations in high-level penetration of distributed-generation systems," *IEEE Trans. Ind. Electron.*, Vol. 60, No. 4, pp. 1417-1428, Apr. 2013.
[31] M. Schweizer and J. W. Kolar, "Design and implementation of a highly efficient three-level T-type converter for low-voltage applications," *IEEE Trans. Power Electron.*, Vol. 28, No. 2, pp. 899-907, Feb. 2013.
[32] L. Zhang, K. Sun, and Y. Fang, "An optimized common mode voltage reduction PWM strategy for T-type three phase three level photovoltaic grid-tied inverter," in *2013 IEEE Energy Conversion Congress and Exposition (ECCE)*, pp. 1623-1627, 2003.
[33] P. Rodriguez, J. Pou, J. Bergas, J. . Candela, R. P. Burgos, and D. Boroyevich, "Decoupled double synchronous reference frame PLL for power converters control," *IEEE Trans. Power Electron.*, Vol. 22, No. 2, pp. 584-592, Mar. 2007.
[34] H.-S. Song and K. Nam, "Dual current control scheme for PWM converter under unbalanced input voltage conditions," *IEEE Trans. Ind. Electron.*, Vol. 46, No. 5, pp. 953-959, Oct. 1999.
[35] A. G. Yepes, A. Vidal, O. Lopez, and J. Doval-Gandoy, "Evaluation of techniques for cross-coupling decoupling between orthogonal axes in double synchronous reference frame current control," *IEEE Trans. Ind. Electron.*, Vol. 61, No. 7, pp. 3527-3531, Jul. 2014.
[36] M. Liserre, F. Blaabjerg, and S. Hansen, "Design and control of an LCL-filter-based three-phase active rectifier," *IEEE Trans. Ind. Appl.*, Vol. 41, No. 5, pp. 1281-1291, Oct. 2005.
[37] V. Ignatova, P. Granjon, and S. Bacha, "Space vector method for voltage dips and swells analysis," *IEEE Trans. Power Deliv.*, Vol. 24, No. 4, pp. 2054–2061, Oct. 2009.
[38] R. Teodorescu, M. Liserre, and P. Rodr Guez, *Grid Converters for Photovoltaic and Wind Power Systems*. Chichester, UK: John Wiley & Sons, Ltd, 2011.

Yuewu Wang was born in Guangxi, China, in 1983. He received his B.S. degree in Instrument Science and Technology from Xi'an Jiaotong University, Xi'an, China, in 2006; and his M.S. degree in Electrical Engineering from Guangxi University, Nanning, China, in 2010. He is currently working toward his Ph.D. degree in Electrical Engineering at the South China University of Technology, Guangzhou, China. His current research interests include pulse

width modulation techniques and grid-connected inverters.

Ping Yang was born in Guangxi, China, in 1967. She received her Ph.D. degree in Control Theory and Engineering from the South China University of Technology, Guangzhou, China, in 1998. She is currently a Professor at the School of Electric Power, South China University of Technology. She is also the Director of the Guangdong Key Laboratory of Clean Energy Technology. Her current research interests include the integration of renewable energy into power system, microgrid control and management, and prediction modeling for wind and solar power.

Zhirong Xu was born in Guangdong, China, in 1989. He received his B.S. degree in Electrical Engineering from the South China University of Technology, Guangzhou, China, in 2013. He is currently working toward his Ph.D. degree in Electrical Engineering at the South China University of Technology. His current research interests include clean energy power generation technology and microgrid energy management.